Supporting Information: Environmentally-Friendly Chemical Time Delays Based on Interrupted Reaction of Reactive Nanolaminates

Shane Q. Arlington,*,†,‡ Joey Chen,† and Timothy P. Weihs*,†,‡

†*Department of Materials Science and Engineering, Johns Hopkins University, 3400 N. Charles St., Maryland Hall 215, Baltimore, MD 21218*

‡*Hopkins Extreme Materials Institute, Johns Hopkins University, Baltimore, MD*

E-mail: arlington@jhu.edu; weihs@jhu.edu

Number of Pages: 12

Number of Figures: 9

Number of Tables: 2

An additional 5 Videos are also available as supporting information.

Freestanding film analysis

We conducted X-ray diffraction (XRD) experiments in a symmetric θ - 2θ configuration on the free-standing foil samples before and after reaction using Cu-Kα radiation (Philips X'Pert) to verify the phases formed. To measure the heat released by the formation reactions across the range of thicknesses and bilayer spacings produced within foil samples, we performed differential scanning calorimetry (DSC) experiments on free-standing foils at 20 $^{\circ}\mathrm{C\,min^{-1}}$ in high purity (99.995%) Ar using a Perkin Elmer DSC 8000.

Since the geometry of the particles is complex, to accurately quantify the ratio of reactive multilayer coating to polymer mesh across the range of coating thicknesses, we measured the densities of the coated meshes. Using this data and measured densities for both the bare polymer and free-standing Al/Ni multilayers, we calculated the volume and mass fraction of Al/Ni within the coated meshes by assuming the coatings have the same density as the free-standing foils. Sample masses for density measurements and DSC measurements were taken using a Mettler Toledo XS3DU microbalance. Volume measurements were made using a Micromeritics AccuPyc II 1340 pycnometer and ultra-high purity (UHP) Helium (99.999%).

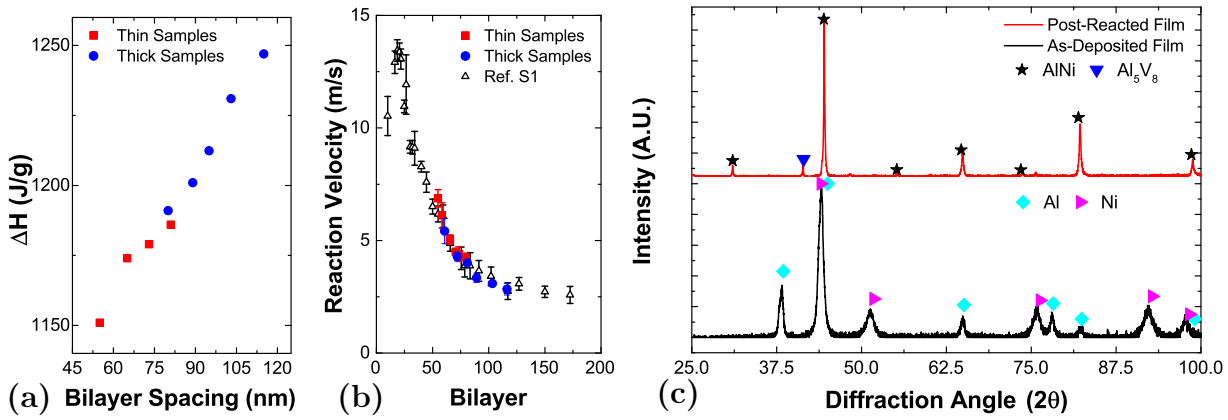

Figure S1: Analysis of free-standing Al/Ni multilayers. **(a)** Heat of reaction (ΔH_r) as a function of bilayer spacing. **(b)** Velocities of free-standing foils. **(c)** X-ray diffraction patterns of as-deposited and post-reacted foils.

As mentioned in the main text, the velocity in the freestanding foils is highest at approx-

imately 7 $\mathrm{m\,s^{-1}}$ for our finest bilayer of 49 nm, and is slowest at 2.8 $\mathrm{m\,s^{-1}}$ for our largest bilayer of 116 nm. Conversely, the heat of reaction is highest for the largest bilayer (1248 $\mathrm{J\,g^{-1}}$) and smallest for the finest bilayer (1150 $\mathrm{J\,g^{-1}}$). These results are fully consistent with prior studies.[S1,S2] As is well explored in the literature, the increase in velocity as the bilayer is refined is attributable to shorter diffusion distances for the reactants allowing for faster heat release, and the commensurate decrease in the heat evolved is due to the increased fraction of intermixed reactants at the Al/Ni interfaces in the as-fabricated state.

Additional coating analysis

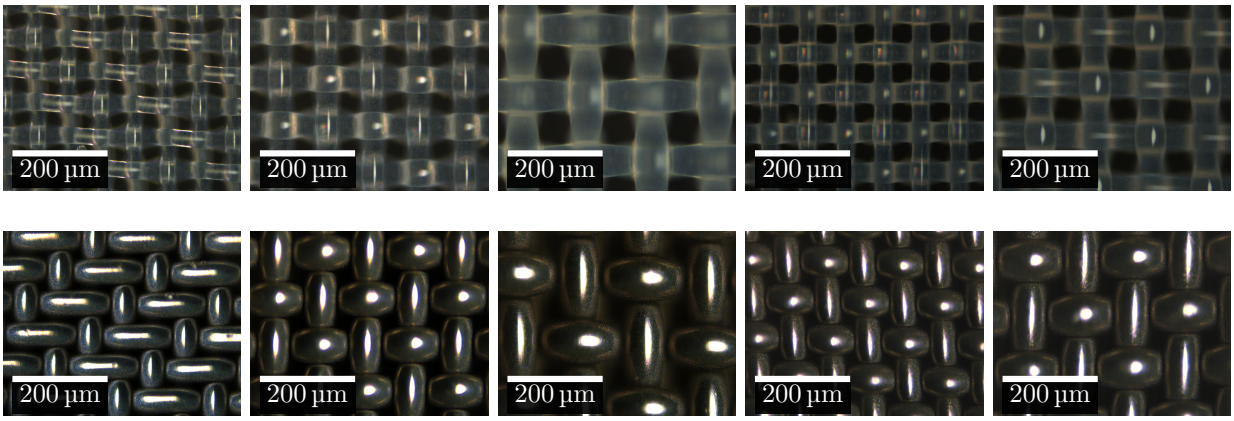

(a) nylon 33 µm (b) nylon 48 µm (c) nylon 65 µm (d) PET 40 µm (e) PET 56 µm

Figure S2: (a)-(e) Optical micrographs of the polymer meshes used in this study before (upper row) and after (bottom row) coating with Al/Ni.

Figure S2 shows micrographs of the meshes used in this study, both as received and with Al/Ni coatings. For each mesh, the mass fraction of the coating can be related to the coating thickness by a second order polynomial, of the form in Equation 1, where M represents the mass of the components and t represents the thickness of the coating. These polynomial fits are shown in Figure S3 **(a)** and **(b)**.

$$\frac{M_{NiAl}}{M_{NiAl} + M_{Mesh}} = at^2 + bt + c \tag{1}$$

A general relationship for the relative volumes of coatings and meshes as a function of coating thickness and mesh diameter was also determined, following the form in Equation 2 and shown in Figure S3. The coefficients for both the individual polynomials and Equation 2 are presented in Table S1, along with the material densities measured via pycnometry used to convert between mass and volume fractions.

$$\frac{V_{NiAl}}{V_{mesh}} = a\frac{t^n d^m}{d^3} \tag{2}$$

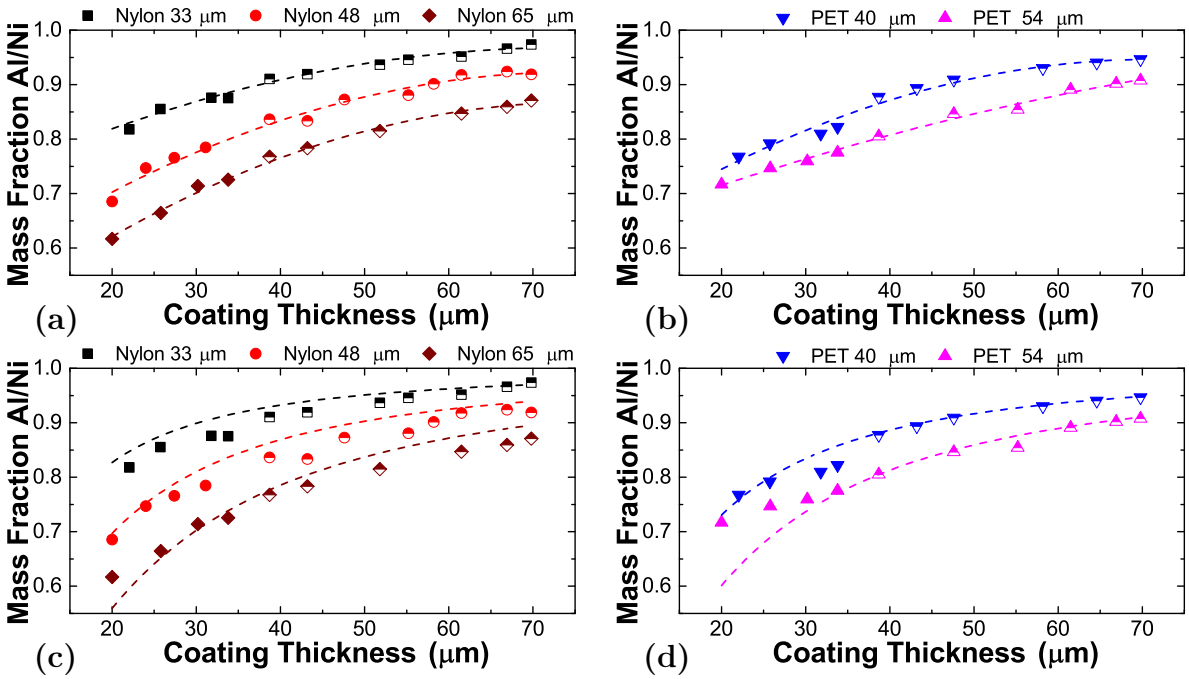

Figure S3: Mass fractions of Al/Ni coatings on **(a)**,**(c)** nylon and **(b)**, **(d)** PET meshes, determined by pycnometry. **(a-b)** Dashed lines show individual second order polynomial fits. **(c-d)** Dashed lines show fitting with Equation 2 and adjusting to mass-fractions by employing material densities.

Multi-rate Propagation

As discussed in the main text, certain samples exhibited multiple reaction rates due to the mesh curling out of plane or disintegrating during reaction, changing the particle to particle contacts and thereby affecting the heat transfer and reaction velocities. Figure S4 shows a

Table S1: Values used in fitting **(a)** mass fractions of Al/Ni coating to individual meshes via second order polynomials, and **(b)** the ratio of volumes of coating to mesh via Equation 2. **(c)** Densities of mesh substrates and Al/Ni coating, as measured by pycnometry.

(a) Individual Polynomial Parameters

Mesh	$a\,(10^{-5}\,\mu m^{-2})$	$b\,(10^{-3}\,\mu m^{-1})$	c
Nylon 33 µm	−5.086	7.539	0.6886
Nylon 48 µm	−7.239	10.89	0.514
Nylon 65 µm	−7.809	11.91	0.4141
PET 40 µm	−7.669	10.93	0.5569
PET 54 µm	−2.370	6.027	0.6042

(b) Equation 2 Parameters

Parameter	Value
a	10.88
m	1.526
n	1.044

(c) Material Densities

Parameter	Value
ρ_{NiAl}	$4.84\,g\,cm^{-3}$
ρ_{PET}	$1.38\,g\,cm^{-3}$
ρ_{Nylon}	$1.14\,g\,cm^{-3}$

plot of the reaction front position (defined by the furthest reacted point along the reaction direction) as a function of time for a mesh that exhibited this behavior, along with frames from the high-speed video spaced at 50 ms intervals. The early propagation occurred with a steady velocity of 11 $mm\,s^{-1}$ until approximately 300 ms, when a region in the upper half of the sample lifted out of plane and curled on itself increasing the velocity to 50 $mm\,s^{-1}$. At just after 500 ms, another small region lifted out and pushed the front forwards at 86 $mm\,s^{-1}$. From 550 ms to 700 ms, the velocity reduced to 18 $mm\,s^{-1}$, close to the early steady value. Finally, after another brief period at 67 $mm\,s^{-1}$, the velocity slowed to 10 $mm\,s^{-1}$ as the reaction front approaches the region of the sample constrained beneath a glass slide, limiting its ability to warp out of plane. Finally (not pictured in the screen shots) the velocity fell to below 5 $mm\,s^{-1}$ as the front moves under the glass slide.

The values shown in Figure S5 represent the overall velocity observed in each sample, including regions where sample flexure or disintegration dramatically changed the propagation velocity. The 33 µm and 48 µm nylon samples were the first sample sets investigated in this study. As we improved the method of sample restraint throughout the study we

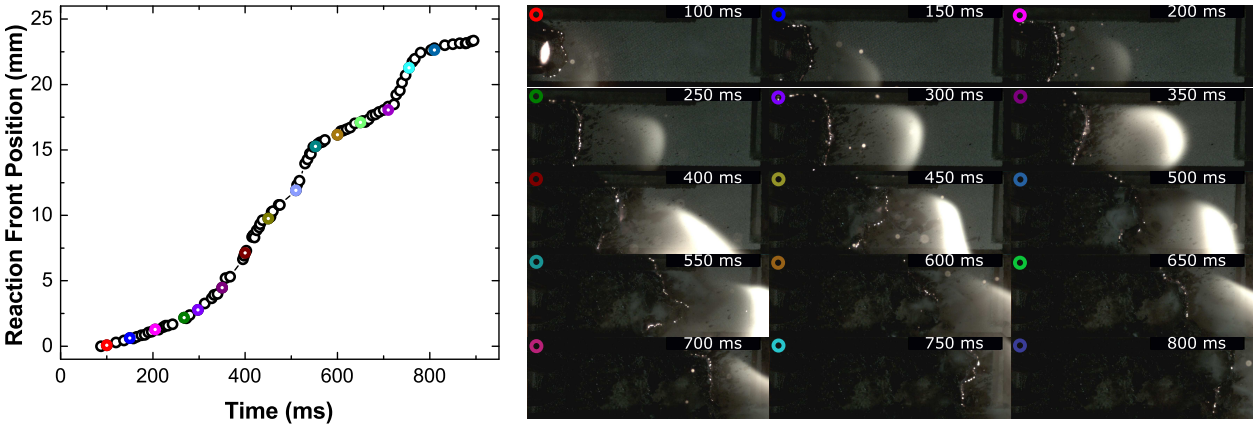

Figure S4: Reaction front position as a function of time, along with a representative montage of images from reaction of a 22 µm coating of Al/Ni on a 48 µm nylon mesh. The frames are spaced evenly by 50 ms increments, and for each frame the corresponding point on the plot is identifiable by the datapoint with its color matching the indicator in the upper left of the frame.

dramatically decreased the incidences of variable propagation velocities, as evidenced by the smaller differences in standard deviations and observed trends between the overall and the steady velocities for the other meshes. On average across all samples, the overall velocity was approximately 10.1% higher than the steady velocities.

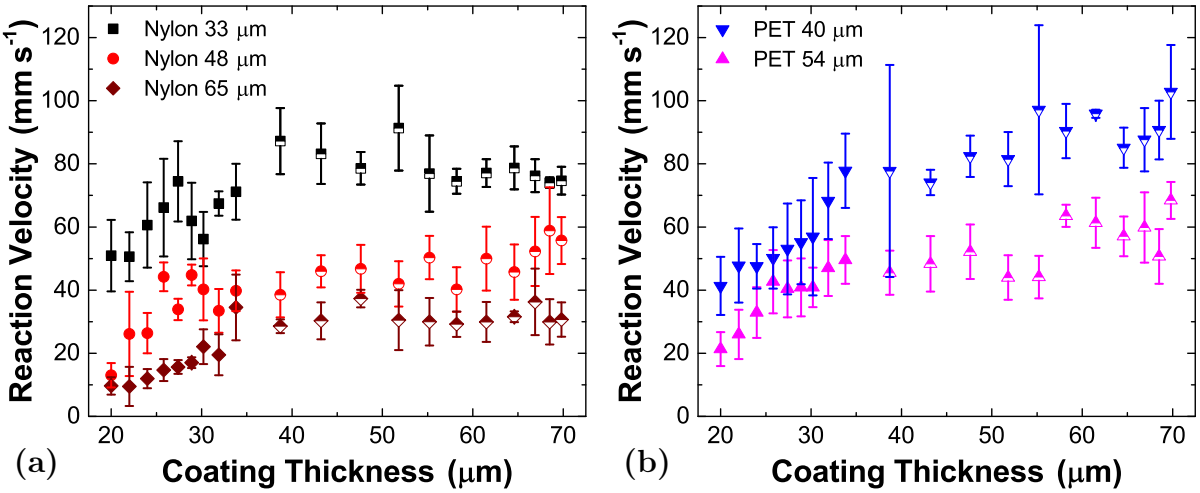

Figure S5: Overall reaction velocities, including unsteady regions, for **(a)** nylon and **(b)** PET meshes taken from overall regression of propagation front versus time. Average values and standard deviations are from at least 3 experiments, with an average N of 5.2.

Microsopics of Reaction: Heating Time Anisotropy

We performed high-magnification video analysis of 40 µm PET meshes due to their low critical coating thickness, which allows us to measure reactions in thin coatings without the mesh disintegrating in the field of view and obscuring the measurements. Using a custom MATLAB code (described in supporting information), we identify the time at which each individual particle ignites. For each particle, the difference in ignition time is compared to each near-neighbor to determine the heating time required for ignition, τ_h, for each particle-particle pair, including both longitudinal heating (in the direction of the propagation front) and transverse heating (normal to the propagation direction) as shown in Figure S6**(c)**. Within each dataset, the heating times to ignite particles oriented vertically (along the transverse direction) and horizontally (along the longitudinal direction) were also considered separately, demonstrating that the particle orientation had little effect on heating times. Figure S6 **(a)** shows characteristic τ_h distributions for thin (22 µm) and thick (69.8 µm) coatings as functions of two factors: the direction of heat flow (measured by the orientation of the particle-particle pairs), and the orientation of the particle being ignited.

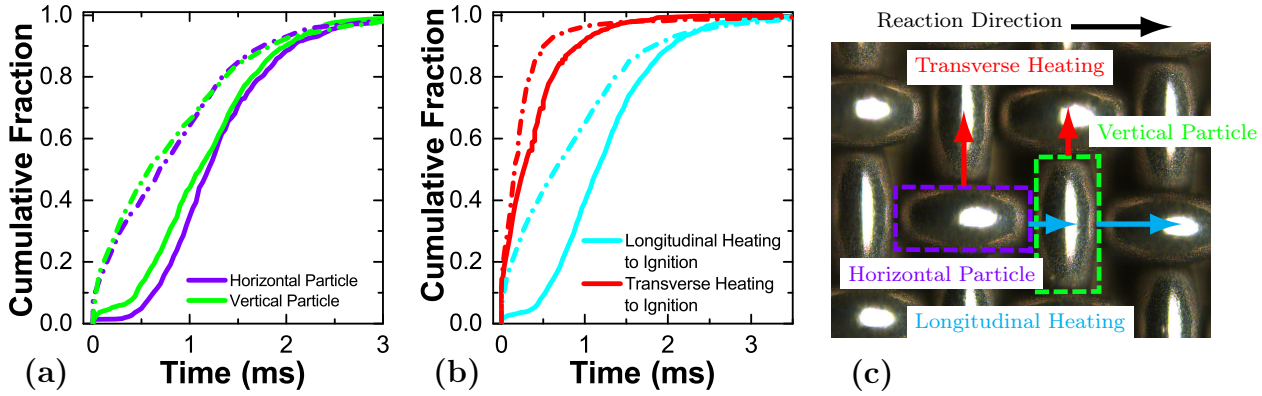

Figure S6: Cumulative probability distribution of heating time to particle ignition, τ_H, as a function of **(a)** orientation of particles being heated longitudinally and (**b**) the direction of heat flow for particles of all orientations. Dashed-dotted curves represent samples with 69.8 µm thick coatings, and solid curves represent samples with 22 µm thick coatings. All data is from coatings on a 40 µm PET mesh. **(c)** Schematic demonstrating longitudinal and transverse heating from both horizontal and vertical particles.

Figure S6 shows only the extrema of the coating thicknessess probed in this study. For the coating thicknesses measured between those extrema, there is a gradual shift of the probability distributions from long times at the thinner coatings to short times at the thicker coatings. In all measurements, the heating times appeared to have relatively little dependence on the orientation of particles being heated, but there is a clear dependence on the orientation of the heat flow which decreases with increasing coating thickness. Particles ignite faster when ignition arises due to heat flow in a direction transverse to the propagation direction, likely because such heat flow is generally coupled with longitudinal heat flow from the propagation front.

Finite Element Analysis

To elucidate how heat transfer affects the ignition delay times in the coated-mesh particle networks, we employed Finite Element Analysis (FEA) to perform transient heat transfer calculations on geometrically simplified models of our coated mesh samples using ANSYS Workbench Mechanical. Figure S7 shows comparisons of the geometry employed in the FEA simulations and the geometry of actual coated mesh samples, as characterized by X-ray Computed Tomography (µCT). The nuanced shape of the particles and their interfaces are simplified in the FEA model, however the scaling of the particle contact area with increasing coating thickness and the mesh wire diameter are consistent with samples measured by µCT.

Several assumptions and simplifications were made in setting up the model. We assigned the particles material properties of the product phase, AlNi, including constant isotropic thermal conductivity[S3] and temperature-dependent values for heat capacity[S4] and coefficient of thermal expansion.[S5] All properties for nylon except the thermal contact conductance were pulled from the ANSYS material database. Properties for PET were taken from ref.[S6] The only heat losses to ambient were due to radiation, with an emissivity of 0.1 - comparable to literature values for polished Al and employed in other studies of Al/Ni nanolaminates.[S7]

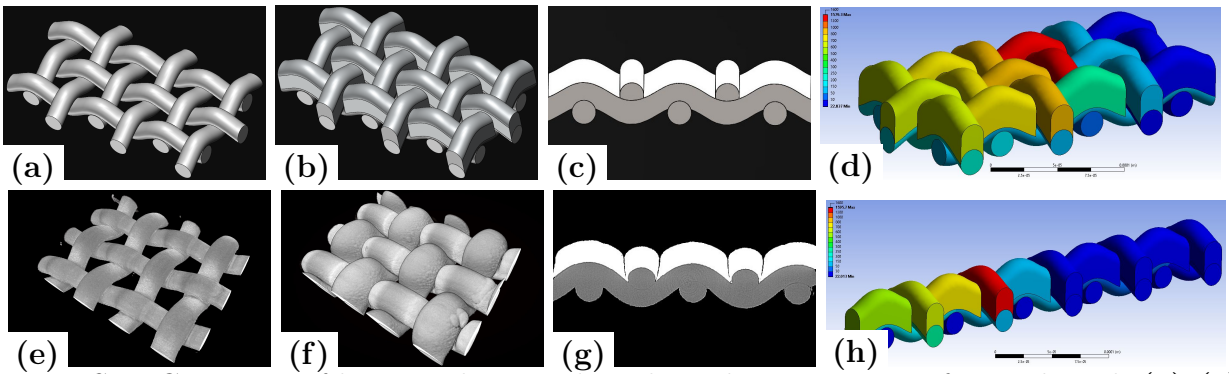

Figure S7: Geometry of bare mesh, coated mesh, and cross section of coated mesh **(a)-(c)** employed in FEA models and **(e)-(g)** reconstructed from µCT data. Screenshots of FEA heat transfer simulations for **(d)** network and **(h)** linear particle models.

Ignition was assumed to be uniform throughout the length of the particle. A parametric study of how wire diameter, d and coating thickness, t, affect heating times was performed using a linear arrangement of particles on nylon mesh strands. This arrangement reduced the heat transfer to one direction and simplified the model and analysis. We performed simulations on networks of particles ranging in size from 2×6 to 6×6 to ensure that the simplified geometry was not significantly affecting the trends observed in the simulations (Figure S8). We observed that networks with an odd width were faster than those with an even width, but that for both odd and even width networks, increasing the overall width decreased the delay times for a given t (Figure S8 **(a)**). We also compared the effect of increasing t for a linear arrangement of particles to a 3×6 network, and determined that the heating times scaled proportionally to t independent of network width (Figure S8 **(b)**). Based on these results, we estimate that a network should be at least 100 particles wide to achieve the observed reaction velocities. Our actual samples ranged from $\approx$ 80 to $\approx$ 150 particles wide. Since the linear geometry allowed for a finer meshing, faster simulations, and simplified analysis, it was used to study the effects of d, t, bilayer spacing λ, and polymer chemistry.

As discussed in the main text, we follow the methods outlined in[S8] and using values for surface roughness, asperity slope, and microhardness provided therein, along with particle

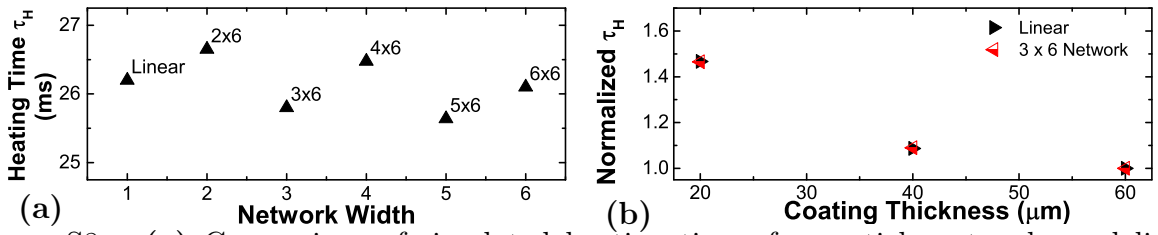

Figure S8: **(a)** Comparison of simulated heating times for particle networks and linear arrangements (20 µm wire with 40 µm thick coating). **(b)** Comparison of trends in heating times (normalized to minimum heating time observed) for a linear arrangement of particles and a 3×6 network on 20 µm wire.

surface roughness determined by cross-sectional SEM, to estimate the thermal contact conductance values of the three interfaces. We estimated the most reasonable values as well as upper and lower bounds of a reasonable range, both presented in Table S2, and performed a parametric analysis across this range centered on the most reasonable estimate. The values are consistent with other literature on rough metal contacts. We performed parametric variations of these values within the determined ranges to ensure that the selected values were reasonable and not dramatically influencing the simulations. As is shown in the main text the selection of the conductance between the metal particles had a significantly larger impact on the results. We selected a value (1250 $\mathrm{W\,m^{-2}\ ^{\circ}C^{-1}}$) which seems reasonable given the expected surface roughness between the particles. We held that value constant in comparing the effects of coating thickness and wire diameter. However, as discussed in the main text, it is expected that the particle to particle conductance value is actually a function of wire diameter and coating thickness as the radius of curvature impacts the deposition at the wire junctions.

For both simulation geometries, the particle(s) at one end started at the maximum reaction temperature T_{max} and the rest of the simulation was set to 22 °C. Via conductive heat transfer, the adjacent particle(s) were heated until the maximum temperature within a particle reached its ignition temperature, T_{ign} at which point the particle 'ignited' and was set to a uniform temperature of T_{max}. To explore the effects of conductance and geometry, T_{ign} was set as 250 °C and T_{max} was set as 1600 °C. For the linear arrangement of particles,

Table S2: Estimated ranges of thermal conductance values and specific values used in FEA simulations to compare effects of coating thickness and wire diameter.

Interface	Conductance Range $\left(\frac{W}{m^{2\circ}C}\right)$	FEA Values $\left(\frac{W}{m^{2\circ}C}\right)$
Particle-Particle	500-1750	1250
Particle-Nylon	20-100	50
Particle-PET	15-60	30
Nylon-Nylon	5-40	15
PET-PET	4-30	10

at least 4 particles were ignited to avoid end effects before determining the ignition time, which was taken as an average of the ignition times of the ignited particles excluding the first. For the network arrangements, the simulation was run until all particles ignited. The ignition time for networks was determined by the total time between ignition of the first particles in each set of adjacent columns, excluding the first and last columns. Constant λ simulations were performed by keeping $T_{ign} = 250\,^{\circ}\text{C}$ and $T_{max} = 1600\,^{\circ}\text{C}$. As discussed in the main text, the effects of λ were probed by varying T_{ign} and T_{max}, both separately and together. A full set of simulations was run for each nylon wire diameter for both a constant λ and with λ varying to mimic the experimental datasets. To more clearly delineate the effect of λ, we also performed a series of simulations with a constant t of 40 µm on a 30 µm nylon wire, with λ varying from 40.6 nm to 96 nm (matching the λ_{avg} in our coatings). The results of those simulations are presented in Figure S9.

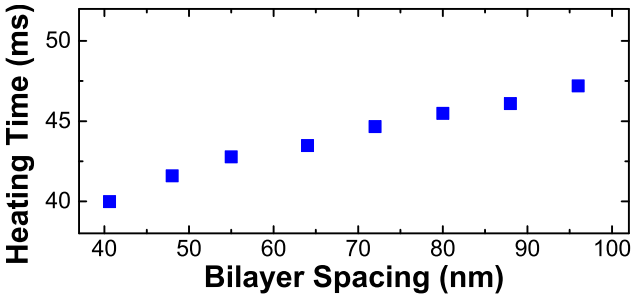

Figure S9: Effect of varying bilayer spacing, λ, with constant coating thickness of 40 µm on a simulated 30 µm diameter nylon mesh.

References

(S1) Knepper, R.; Snyder, M. R.; Fritz, G. M.; Fisher, K.; Knio, O. M.; Weihs, T. P. Effect of varying bilayer spacing distribution on reaction heat and velocity in reactive Al/Ni multilayers. *J. Appl. Phys.* **2009**, *105*, 083504.

(S2) Gavens, A. J.; Van Heerden, D.; Mann, A. B.; Reiss, M. E.; Weihs, T. P. Effect of intermixing on self-propagating exothermic reactions in Al/Ni nanolaminate foils. *J. Appl. Phys.* **2000**, *87*, 1255.

(S3) Terada, Y.; Ohkubo, K.; Nakagawa, K.; Mohri, T.; Suzuki, T. Thermal conductivity of B2-type aluminides and titanides. *Intermetallics* **1995**, *3*, 347–355.

(S4) Wei, C.; Nesterenko, V.; Weihs, T.; Remington, B.; Park, H.-S.; Meyers, M. Response of Ni/Al laminates to laser-driven compression. *Acta Mater.* **2012**, *60*, 3929–3942.

(S5) Wang, Y.-K.; Liu, Z.; Chen, L.-Q. Thermodynamic properties of Al, Ni, NiAl, and Ni3Al from first-principles calculations. *Acta Mater.* **2004**, *52*, 2665–2671.

(S6) Lopes, C. M. A.; Felisberti, M. I. Thermal conductivity of PET/(LDPE/AI) composites determined by MDSC. *Polym. Test.* **2004**, *23*, 637–643.

(S7) Grapes, M. D.; Weihs, T. P. Exploring the reaction mechanism in self-propagating Al/Ni multilayers by adding inert material. *Combust. Flame* **2016**, *172*, 105–115.

(S8) Babu, K. N. Thermal Contact Resistance: Experiments and Simulation. Masters Thesis, Chalmers University of Technology, 2015.